

PAPER • OPEN ACCESS

Lattice strain and texture development in coarse-grained uranium – a neutron diffraction study

To cite this article: P Earp *et al* 2018 *J. Phys.: Conf. Ser.* **1106** 012012

View the [article online](#) for updates and enhancements.



IOP | ebooks™

Bringing you innovative digital publishing with leading voices
to create your essential collection of books in STEM research.

Start exploring the **collection** - download the first chapter of
every title for free.

Lattice strain and texture development in coarse-grained uranium – a neutron diffraction study

P Earp^{1,4}, S Kabra², J Askew³ and T J Marrow¹

¹ Department of Materials, University of Oxford, Parks Road, Oxford, OX1 3PH, UK

² ISIS Neutron and Muon Source, Science and Technology Facilities Council, Rutherford Appleton Laboratory Didcot, OX11 0QX, UK

³ AWE plc, Aldermaston, Reading, Berkshire, RG7 4PR, UK

philip.earp@materials.ox.ac.uk

Abstract. A neutron diffraction study of deformation in a cast uranium has been conducted for the first time. Lattice-scale plasticity in this coarse-grained material initiates at a lower stress than in a previous study of fine-grained material in the literature. This is attributed to a combination of larger thermal residual stresses in the coarse-grained material and the Hall-Petch effect making twinning easier in large grains. Asymmetry between the tensile and compressive response shows that twinning is the dominant plastic deformation mechanism at low strains. Axial texture changes for the cast uranium were calculated by post processing of the full diffraction spectra, which shows that lattice rotations associated with twinning occurred at yield. This lattice rotation was observed to disappear after unloading, which indicates that de-twinning can occur in uranium. ©British Crown Owned Copyright 2018/AWE

1. Introduction

Understanding fracture processes in materials such as cast alpha-uranium is a complex task; the combined effects of large grains [1], residual stresses and anisotropic mechanical properties creates unusual responses to deformation, and variable mechanical properties [2,3].

Uranium metal is highly elastically anisotropic, both elastically and plastically. In the room temperature alpha phase it has an orthorhombic crystal structure [4,5], an anisotropic coefficient of thermal expansion [6], and each grain has a limited number of slip modes; in particular, there are no active slip modes at room temperature to accommodate deformation perpendicular to the (001) plane [7]. Consequently, it deforms extensively by twinning, the cooperative shear of sections of the crystalline lattice, with (130) and '(172)' twins commonly observed [8]. Incompatibilities between deforming grains can result in stress concentrations that may initiate fracture. To fully understand local processes such as fracture, there is a need to develop models, such as the crystal plasticity finite element (CPFE) method, which can be used to predict the strength of engineering components whilst incorporating the internal microstructure of the material. A number of visco-plastic self-consistent (VPSC) modelling schemes have been developed for fine-grained wrought uranium grains [9] which has then been incorporated into a finite element framework [10] which was then used to model compressive and rolling deformation. Uranium presents unique challenges to the CPFE modelling

⁴ Author to whom any correspondence should be addressed



community, specifically how to incorporate the effects of twins into a dislocation-based model [11], and how to experimentally validate these models in coarse-grained microstructures.

This paper presents results from a neutron diffraction experiment with measurements performed on coarse-grained cast uranium under tension and compression. Analysis is performed using both single-peak fitting and Rietveld refinement, with a focus on lattice strain accumulation and texture changes due to the applied deformation.

2. Experimental methods

2.1. The *ENGIN-X* Diffractometer

The neutron diffraction experiment was performed at the *ENGIN-X* beamline [12], ISIS Neutron Source, Rutherford Appleton Laboratory, UK under experiment number 1710227. The specimen is held between the grips of a horizontally mounted 100 kN Instron servo-hydraulic stress rig at an angle of 45° to the incoming beam direction, and two neutron detector banks are located as shown in figure 1. Bank 1 can measure changes in lattice spacing in the family of grains that have diffracting plane normals parallel to the loading axis and detector bank 2 measures in the orthogonal direction. The diffracting gauge volume is defined by slits and radial collimators positioned in front of the detectors.

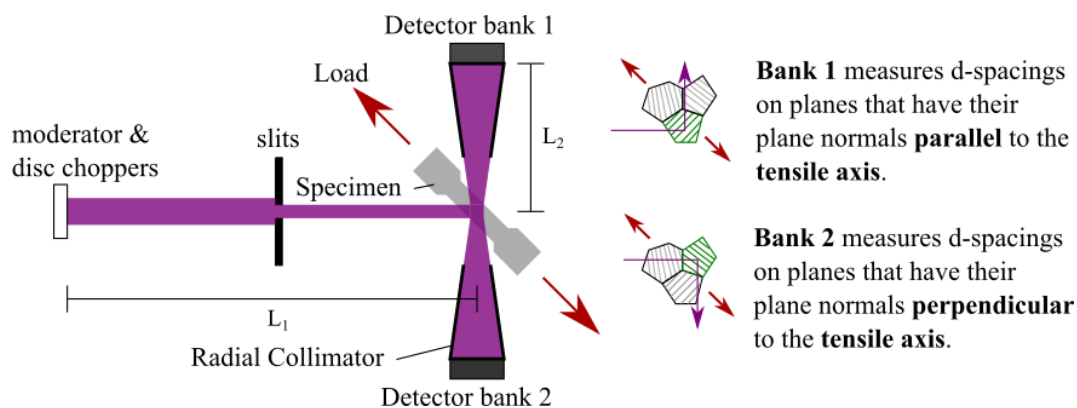


Figure 1. Schematic plan view of the *ENGIN-X* beamline at the ISIS neutron source.

2.2. Specimen design and microstructural characterisation

The depleted uranium was provided by AWE plc (UK) as a cast plate; the material contained many carbides.

The tensile specimens had a gauge diameter of 8.00 mm and a parallel gauge length of 31.42 mm, and the compression specimens a 14.00 mm diameter and 28.00 mm.

Grip extensions (HSLA steel) reduced the potential risk of material transfer to the *ENGIN-X* stress rig grips. In order to satisfy the radiation protection requirements, a conventional strain gauge could not be attached to the specimens, and the gauge region of each specimen was wrapped in aluminium foil to reduce the risk of contamination if the sample were to fracture. Digital image correlation was therefore used to measure the displacement of the sample grips at each stage of the test. The total strain was calculated from the relative displacement in the horizontal x-direction (parallel to the loading axis) of the moving grip with respect to the fixed grip using a gauge length equal to the specimen length between the grips.

The material's microstructure was investigated using scanning electron microscopy (SEM) and electron backscatter diffraction (EBSD). Cuboid specimens ($6\text{ mm} \times 6\text{ mm} \times 1.5\text{ mm}$) from the same cast plate were prepared by grinding and polishing to $3\mu\text{m}$ diamond, then electropolished at 12V, 0.4A for 5 minutes using a 10:6:6 volumetric ratio of ethanol, orthophosphoric acid and ethylene glycol as the electropolishing solution [13]. The EBSD analysis obtained 8 scans, each approximately $3\text{ mm} \times 1.5\text{ mm}$, that together form a large area map (figure 2). The grains are clustered into areas of similar

orientation with approximately 5° misorientations between the grains in a cluster and a larger misorientation of greater than 30° between the clusters. The average grain size within a cluster is approximately $200\ \mu\text{m}$ whilst the clusters are $> 4\ \text{mm}$ in size.

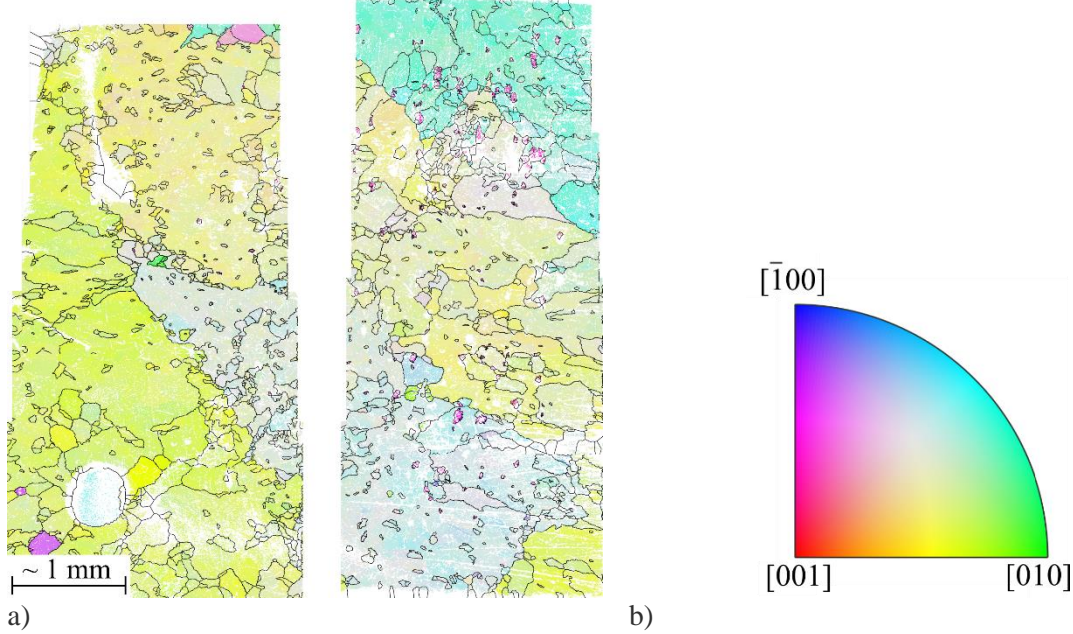


Figure 2. Stitched EBSD orientation maps (a) showing a representative microstructure of the uranium metal used in this experiment. Each grain is coloured according to its crystal orientation with respect to the out-of-plane direction, shown in the inverse pole figure (b). Thin black lines are drawn along boundaries with misorientation greater than 3° .

2.3. Neutron diffraction experiment

Sample T1 was strained in load-control in steps of $\sim 10\ \text{MPa}$, from a pre-load of $2\ \text{MPa}$ up to a maximum load of $310\ \text{MPa}$ with a neutron diffraction measurement taken at each step (each requiring ~ 25 minutes). The gauge volume of $4\ \text{mm} \times 4\ \text{mm} \times 8\ \text{mm}$ sampled approximately 16000 grains.

Sample T2 was tested in the same manner, but the load steps were adjusted to better capture the elastic-plastic transition, after performing the measurement at maximum load, the specimen was to $10\ \text{MPa}$ for a final measurement.

From a compressive pre-load of $-4\ \text{MPa}$, sample C1 was loaded in steps of $-10\ \text{MPa}$ to $-310\ \text{MPa}$, followed by an unloaded measurement at $-10\ \text{MPa}$. The gauge volume of $4\ \text{mm} \times 4\ \text{mm} \times 12\ \text{mm}$ sampled approximately 24000 grains.

2.4. Data processing methodology

Initial processing of the experimental data used the ENGIN-X OpenGenie software [14] to perform single-peak fits. Lattice strains for a reflection $\{hkl\}$, ϵ^{hkl} , were calculated from the measured d-spacing using equation 1 where the reference lattice, d_0^{hkl} , is the value in the initial unloaded state.

$$\epsilon^{hkl} = \frac{d^{hkl} - d_0^{hkl}}{d_0^{hkl}} \quad [1]$$

A Rietveld refinement method in the GSAS software package [15] was used to fit multi-peak profiles to the measured spectra. This fits parameters including the lattice parameters, peak shape, and peak intensity (sample texture) to the entire spectrum at once.

Quantifying the ratio between the measured intensity in a $\{hkl\}$ reflection, and the $\{hkl\}$ peak intensity expected from a random distribution of grains, gives a measure of texture along the diffraction vector, in units of multiples of random distribution (MRD). The preferred orientation correction factor

quantifies this, and is calculated from the coefficients of the 10th order spherical harmonic function fitted as part of the Rietveld refinement. The values of this factor as a function of crystal direction were plotted on an inverse pole figure using the ‘SMARTSinvpol’ script [16].

Lattice parameter strains, ε_a , ε_b , and ε_c were calculated from the lattice parameters a , b , and c using equation 2, where a_0 , b_0 , and c_0 are the lattice parameters measured at pre-load.

$$\varepsilon_a = \frac{a - a_0}{a_0} \quad \varepsilon_b = \frac{b - b_0}{b_0} \quad \varepsilon_c = \frac{c - c_0}{c_0} \quad [2]$$

Each diffraction peak $\{hkl\}$ contains contributions from the family of grains that have their $\{hkl\}$ planes oriented in the diffraction condition (that is their $\{hkl\}$ plane-normals parallel or perpendicular to the loading axis for detector banks 1 and 2 respectively). The measured $\{hkl\}$ lattice strain is therefore proportional to the average stress on that family of grains [17].

3. Results

3.1. Macroscopic flow curve

The macroscopic flow curve for the coarse-grained samples (CG T1, CG T2, and CG C1) are plotted in figure 3 along with data from a fine-grained rolled uranium deformed along the rolling direction (FG RD) and transverse direction (FG TD) from Brown et al. [17]. The random error in the strain was estimated from the standard deviation in the DIC-measured displacements to be on the order of 0.05 %. This assumes that the grips do not themselves deform, so the total strain for the coarse-grained samples is only indicative and should not be used for detailed comparison with the data from the fine-grained uranium. The elastic modulus of the material varies with orientation and is therefore not known exactly in these coarse-grained specimens, however its value must lie between the maximum and minimum single crystal moduli of 288 GPa and 149 GPa, indicated on figure 3 as a pair of straight dotted lines. The flow curves all have a very small linear elastic region, with non-linearity observed from approximately 70 MPa in tension and 30 MPa in compression.

3.2. Lattice strain development

Figure 4 shows the development of lattice strains measured with the bank 1 detector (diffraction vector parallel to the loading direction), as a function of applied stress. Lattice strains from fine-grained uranium deformed in tension along the rolling direction [17] is shown for comparison. There is a clear similarity in the lattice strain response between the 2 specimens deformed in tension. A linear behaviour was observed during loading from the pre-loaded state until a critical stress at which the $\{200\}$ and a -strains begin to saturate with further increases in stress resulting in no additional lattice strain on these planes. This critical stress occurs at 90 MPa for specimen T1 and 110 MPa for specimen T2. The gradients of the ε_a , ε_b , and ε_c in the elastic region are (244 ± 8) GPa, (236 ± 13) GPa, and (224 ± 8) GPa for specimen T1 and (276 ± 8) GPa, (198 ± 3) GPa, and (220 ± 7) GPa for specimen T2. In compression, the lattice parameter and single-peak strains respond linearly with applied stress up to 130 MPa, a higher threshold stress than in tension. The lattice parameter moduli for specimen C1 are (191 ± 3) GPa, (201 ± 2) GPa, and (192 ± 4) GPa for a , b and c respectively.

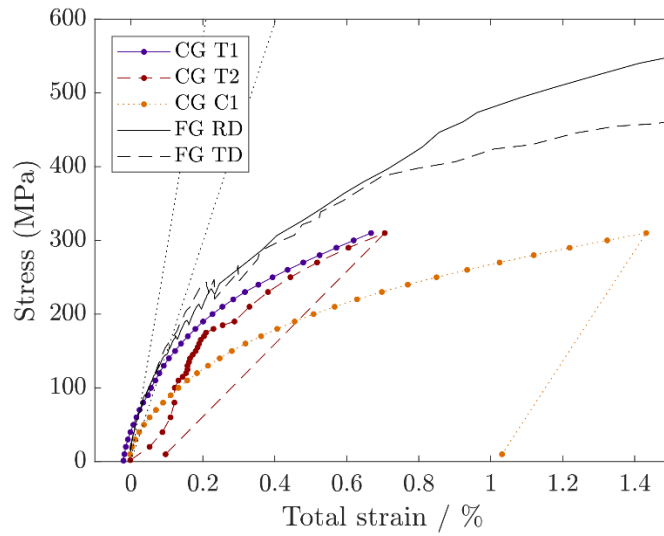


Figure 3. Plot of applied stress against total strain. Lines labelled CG are from the coarse-grained material tested in this experiment, with strain measured using DIC. Lines labelled FG are from fine-grained rolled material tested by Brown et al. [17] using a conventional extensometer for strain measurement. The two straight dotted lines represent the maximum and minimum possible young's moduli for an alpha-uranium polycrystal of 288 GPa and 149 GPa.

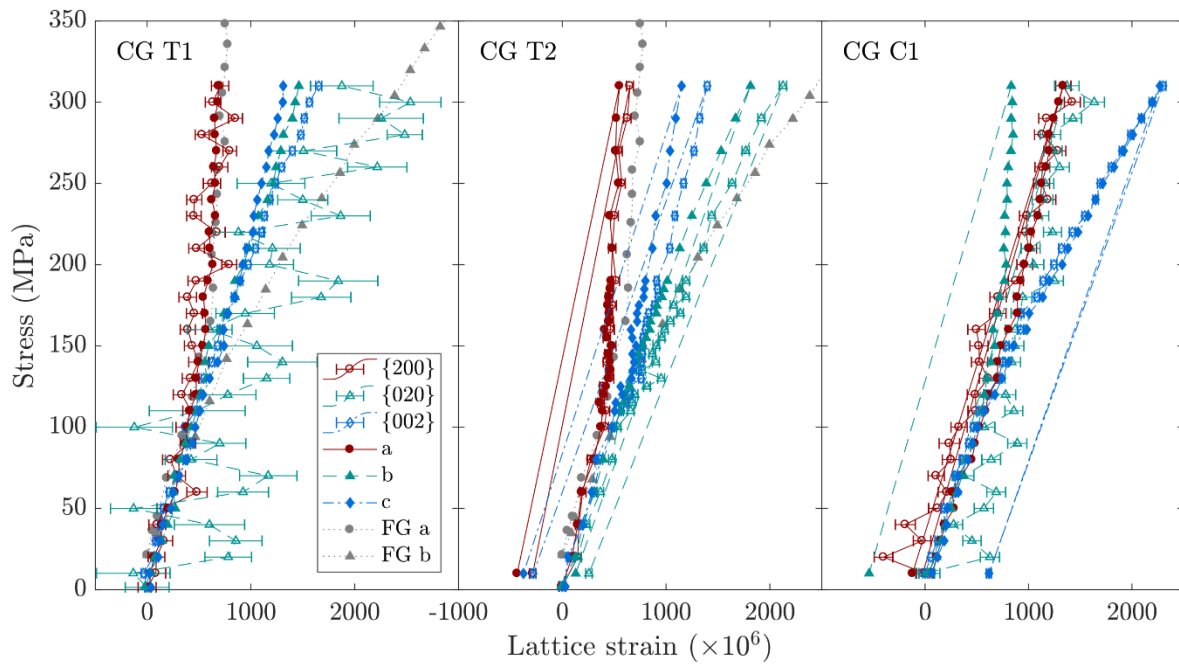


Figure 4. Lattice strain development as a function of applied stress. Open markers represent single-peak lattice strains whilst filled markers represent lattice parameter strains measured from the Rietveld refinement.

3.3. Texture changes

3.3.1. Inverse pole figures

Figures 5a, 5b, 5c, and 5d are inverse pole figure representations of the sample texture as calculated from the Rietveld refinement with the samples in their pre-load state. There are two preferred orientations in sample T1; the predominant orientation is where the loading direction is parallel to $\{115\}$ plane normals ($n_{\{115\}}$), and the secondary orientation is where it is parallel to $n_{\{312\}}$. Sample T2 has a uniaxial texture, with most grains in the gauge volume having $n_{\{020\}}$ parallel to the loading direction. Sample C1 has two predominant families of planes in the diffraction condition; $\{190\}$, the peak closest to $\{010\}$ in the inverse pole figure, and $\{350\}$, the peak situated halfway between $\{010\}$ and $\{100\}$.

Figures 5e, 5f, and 5g show the absolute change in texture, in MRD, between the initial pre-load state, and the state at maximum tensile or compressive load. A positive value in a particular crystal direction on the inverse pole figure corresponds to an increase in the volume of grains oriented with the diffraction vector (the loading direction) parallel to that particular crystal direction. Figure 5h shows the error in the values presented in figure 5e (sample T1 at maximum tensile load). The inverse pole figure representation of the error was calculated by propagation of the errors in the spherical harmonic coefficients. Sample T1 shows an increase in texture in the upper sector of the inverse pole figure, with a maximum increase of around 0.3 MRD close to $\{171\}$, and a decrease of similar magnitude close to $\{115\}$. In sample T2, an increase in texture close to $\{100\}$ is accompanied with slight decreases near $\{024\}$. The decrease visible near to $\{010\}$ is of a similar magnitude to the error shown in figure 5h. Sample C1 shows an increase in intensity of 0.4 MRD parallel to the $\{310\}$ plane normal and an equivalent decrease parallel to $\{350\}$.

Figures 5i and 5j show the absolute change in texture between the initial pre-load state and the state at unload at the end of the experiment for samples T2 and C1. No unload was performed for specimen T1. The texture of sample T2 after unload is almost identical to its initial state; the texture change that was present at maximum load has disappeared. Sample C1 however shows very similar textures at maximum load and after unloading, with no significant change during unloading.

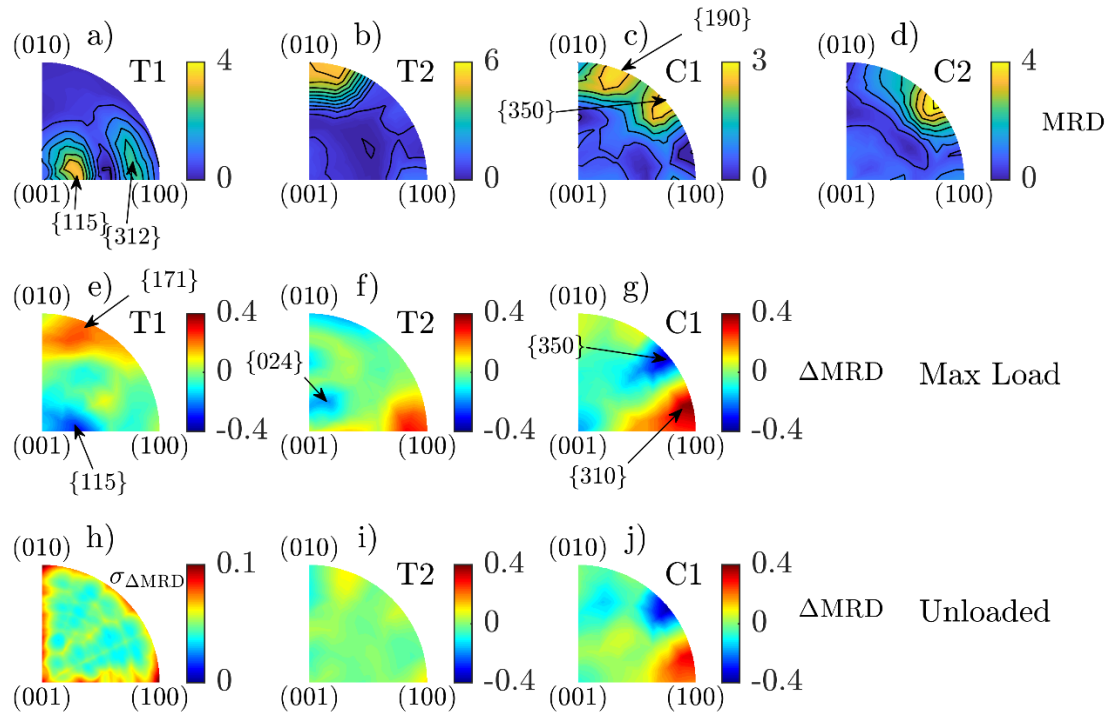


Figure 5. a-d: Axial texture in the loading direction under pre-load, calculated by Rietveld refinement, for specimens T1, T2, C1 and C2. Plotted as inverse pole figures (IPFs) in multiples of random distribution (MRD). Higher values represent a strong texture, i.e. a preferred orientation. e-g: Absolute change in texture, in MRD, between pre-load and maximum load state. i-j: Absolute change in texture, in MRD, between pre-load and final unloaded state. h: Error in values presented in figure 5e, calculated from errors in the fitted spherical harmonic coefficients. Representative of errors in all differential texture measurements e-g and i-j.

4. Discussion

4.1. Macroscopic response and lattice strains

The gauge volume for neutron measurement is considerably smaller than the total sample size, and deformation in a region outside of the gauge volume will contribute to the total strain even if the gauge region is still behaving elastically. That there is still an elastic region to the stress vs. lattice strain plot in figure 4 shows that plasticity is not initiating in all grains at the start of the test, therefore there must be residual stresses such that a subset of grains are already at their yield point to give the non-linear macroscopic flow curve.

Such high residual stresses are indeed possible when we consider the processing route of the coarse-grained material. During the casting process, after solidification, the sample undergoes a solid-state transformation from the beta phase to the orthorhombic alpha phase [18] and large thermal stresses are built up due to the thermal expansion between neighbouring grains [6]. It is well known that these stresses are large enough to cause plastic deformation; thermal cycling of textured uranium causes significant shape change known as ‘thermal cycling growth’ [19]. In this material, the small grains comprising the larger clusters are all oriented in similar directions, so large contiguous volumes could be at the yield stress in the initial unloaded state. The stress at which the lattice parameter strains in figure 4 deviate from linearity is the lattice yield stress. In both tensile specimens it is the a-parameter that saturates, and the lattice yield stress is lower than in the fine-grained material. This effect is most pronounced in the specimen T2 where yield occurs approximately 30 MPa earlier than for the fine-grained material. This would be expected from a Hall-Petch-type grain size effect [20].

4.2. Texture changes

The measured texture in the gauge volume of each sample is very strong, with only one or two clusters of orientations present in each case. An increase in texture in one direction is seen alongside a decrease in another direction. Since the production of a twin reduces volume fraction of parent material and increases the volume fraction of material in the twin orientation, the directions of positive and negative texture changes can be assigned to the parent and twin orientations respectively.

At the small applied strains in this test, lattice rotation due to dislocation slip is negligible. The observed texture changes are therefore related to the formation of deformation twins. The twin is effectively a new grain in a different orientation, so the formation of twins will be associated with a texture decrease in the parent orientation and an increase in the twin orientation. The twin has a fixed misorientation with the parent grain that depends on the active twinning variant; the variant is dependent on the local stress condition via the Schmid factor [21].

5. Conclusion.

The macroscopic yield point in the deformation of cast uranium in tension and compression is ill-defined, due to large residual stresses.

Despite significant texture differences, very similar macroscopic and lattice-strain response was seen in deformed in tension, with saturation of the a/{200} strains. The specimen deformed in compression responded differently, with saturation of the b-parameter strains only. The asymmetry between tensile and compressive response suggests twinning is the dominant deformation mechanism.

The texture affects the active twinning systems in a particular volume, however the exact identification of the active twin variant was not possible from axial texture measurement only. Large grains make the interpretation of the data difficult and any future experiment would have to include a larger neutron gauge volume in order to provide a more representative measurement of the whole-sample response.

Acknowledgments

The authors thank the Science and Technology Facilities Council for beamtime at the ISIS Neutron and Muon Source under experiment 1710227, as well as the facility staff, in particular Dr Joe Kelleher for experiment planning and Dr Marek Jura for radiation protection advice. Thanks are extended to Dr Keith

Hallam and Dr Chris Jones at the Interface Analysis Centre, University of Bristol, for help with the EBSD mapping, and to Bjorn Clausen and Don Brown at Los Alamos National Laboratory, USA, for assistance with Rietveld refinement. We acknowledge the assistance of Dr Dong Liu, Talha Pirzada and Shixiang Zhao from the University of Oxford during the neutron diffraction experiment.

References

- [1] Sarel J, Pelleg J and Kimmel G, 1986 Evaluation of Anisotropy in Cast and Heat Treated "Adjusted-Uranium." *Journal of Nuclear Materials* **140** 288–92
- [2] Olofson CT, Meyer GE and Hoffmann AL, 1976 *Processing and Applications of Depleted Uranium Alloy Products*. (Columbus, OH, USA: Battelle Columbus Laboratories)
- [3] Caskey Jr GR, 1959 *Mechanical Properties of Uranium Plate*. (Savannah, GA: E. I. Du Pont de Nemours & Co.)
- [4] Jacob CW and Warren BE, 1937 The Crystalline Structure of Uranium. *Journal of the American Chemical Society* **59** 2588–91
- [5] Cahn RW, 1953 Plastic Deformation of Alpha-Uranium ; Twinning and Slip. *Acta Metallurgica* **1** 49–70
- [6] Frost BRT, 1994 *Nuclear Materials - Materials Science and Technology Volume 10A*
- [7] Daniel JS, Lesage B and Lacombe P, 1971 The influence of temperature on slip and twinning in uranium. *Acta Metallurgica* **19** 163–73
- [8] McCabe R, Field R, Brown D, Alexander D and Cady C, 2008 Electron Backscatter Diffraction (EBSD) Characterization of Twinning Related Deformation and Fracture in α -Uranium. *Microscopy and Microanalysis* **14** 638–9
- [9] Zecevic M, Knezevic M, Beyerlein IJ and McCabe RJ, 2016 Origin of texture development in orthorhombic uranium. *Materials Science and Engineering: A* **665** 108–24
- [10] Zecevic M, Knezevic M, Beyerlein IJ and McCabe RJ, 2016 Texture formation in orthorhombic alpha-uranium under simple compression and rolling to high strains. *Journal of Nuclear Materials* **473** 143–56
- [11] Ardeljan M, McCabe RJ, Beyerlein IJ and Knezevic M, 2015 Explicit incorporation of deformation twins into crystal plasticity finite element models. *Computer Methods in Applied Mechanics and Engineering* **295** 396–413
- [12] Santisteban JR, Daymond MR, James JA and Edwards L, 2006 ENGIN-X: A third-generation neutron strain scanner. *Journal of Applied Crystallography* **39** 812–25
- [13] Jones CP, Scott TB and Petherbridge JR, 2015 Structural deformation of metallic uranium surrounding hydride growth sites. *Corrosion Science* **96** 144–51
- [14] Akeroyd FA, Ashworth RL, Campbell S, Johnston SD, M Moreton-Smith C, Sergeant RG, et al., 2018 Open Genie Reference Manual - Version 2.0
- [15] Larson AC and Von Dreele RB, 2004 General Structure Analysis System (GSAS). *Los Alamos National Laboratory Report LAUR* **86** 748
- [16] Clausen B, 2003 *SMARTSware manual*. (Los Alamos National Laboratory, NM, USA)
- [17] Brown DW, Bourke M a M, Clausen B, Korzekwa DR, Korzekwa RC, McCabe RJ, et al., 2009 Temperature and direction dependence of internal strain and texture evolution during deformation of uranium. *Materials Science and Engineering A* **512** 67–75
- [18] McCabe RJ, Capolungo L, Marshall PE, Cady CM and Tomé CN, 2010 Deformation of wrought

uranium: Experiments and modeling. *Acta Materialia* **58** 5447–59

- [19] Kelman LR, 1949 Dimensional changes in Uranium Under Thermal Cycling. *Journal of Metallurgy and Ceramics* **4**
- [20] Meyers MA, Vöhringer O and Lubarda VA, 2001 The onset of twinning in metals: A constitutive description. *Acta Materialia* **49** 4025–39
- [21] Godet S, Jiang L, Luo AA and Jonas JJ, 2006 Use of Schmid factors to select extension twin variants in extruded magnesium alloy tubes. *Scripta Materialia* **55** 1055–8